

Kinematics from spectroscopy with a wide slit: detecting black holes in galaxy centres

Witold Maciejewski and James Binney

Theoretical Physics, 1 Keble Road, University of Oxford, Oxford, OX1 3NP

30 October 2018

ABSTRACT

We consider long-slit emission-line spectra of galactic nuclei when the slit is wider than the instrumental PSF, and the target has large velocity gradients. The finite width of the slit generates complex distributions of brightness at a given spatial point in the measured spectrum, which can be misinterpreted as coming from additional physically distinct nuclear components. We illustrate this phenomenon for the case of a thin disc in circular motion around a nuclear black hole (BH). We develop a new method for estimating the mass of the BH that exploits a feature in the spectrum at the outer edge of the BH’s sphere of influence, and therefore gives higher sensitivity to BH detection than traditional methods. Moreover, with this method we can determine the black hole mass and the inclination of the surrounding disc separately, whereas the traditional approach to black-hole estimation requires two long-slit spectra to be taken. We show that with a given spectrograph, the detectability of a BH depends on the sense of rotation of the nuclear disc. We apply our method to estimate the BH mass in M84 from a publicly available spectrum, and recover a value 4 times lower than that published previously from the same data.

Key words: instrumentation: spectrographs — methods: data analysis — techniques: spectroscopic — galaxies: nuclei — galaxies: individual:M84 — galaxies: kinematics and dynamics

1 INTRODUCTION

Long-slit spectroscopy has been for decades a fundamental tool of astronomy, and although integral-field spectrographs are now beginning to be important for ground-based observations of galactic dynamics (e.g., SAURON, Copin et al. 2000), the Hubble Space Telescope (HST) has never been more reliant on long-slit spectroscopy.

Observations with long-slit spectrographs often use a slit that is wider than the FWHM of the instrumental point-spread-function (PSF). This practice is conventionally considered to enhance the signal-to-noise ratio (S/N) of the data at the price of what may be an insignificant loss in velocity resolution. Here we show that when the target has steep velocity gradients, the use of a wide slit can have more subtle effects, because the position and velocity information becomes entangled along the dispersion direction. If these effects are not recognized in the data, a misleading impression of the structure of the target can be inferred. When the effects of a wide slit are recognized, however, they can increase the diagnostic power of the spectrum over that of a narrow-slit spectrum of equal S/N.

Since our study has been motivated by a programme of spectroscopy of galactic nuclei using the STIS instrument

on HST (Marconi et al. 2000; Axon et al. 2000), we focus on the specific case of STIS spectra of gas swirling around a black hole in a galactic nucleus. However, the principles we elucidate have a wider applicability: whenever an object with steep velocity gradients is studied with a slit that is wider than the FWHM of the PSF. Large velocity gradients occur in shocks and contact discontinuities, as well as in accretion discs around black holes.

In Section 2 we analyze the appearance of galactic-disc spectra that are taken with a slit that is much wider than the PSF and has been laid along the disc’s line of nodes. In Section 3 we use this analysis to develop a new estimator for the mass of the nuclear BH. In Section 4 we generalize the analysis of Sections 2 and 3 to a slit that is inclined to the line of nodes. We find that, paradoxically, the detectability of a BH with a given spectrograph depends on the sense of rotation of its accretion disc. We also investigate the case of a slit that does not pass through the nucleus. In Section 5 we consider the case in which the FWHM of the PSF is comparable to the slit width. In Section 6 we reanalyse STIS observations of M84 taken by Bower et al (1998), and show that the results of Section 4 enable us to understand these data with a much simpler model of the galaxy than that developed by Bower et al., and yield a mass for the black

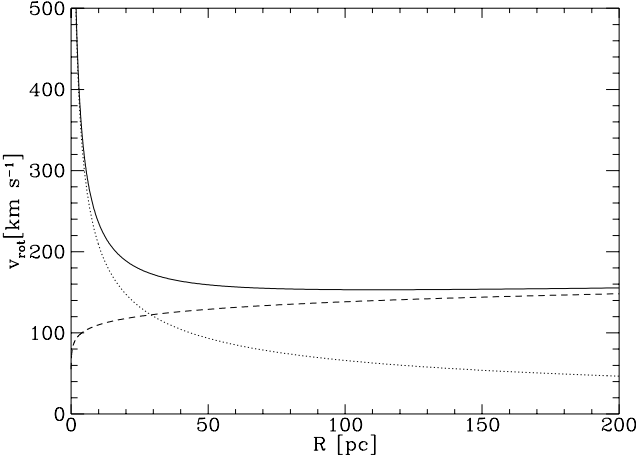


Figure 1. Circular-speed curves for the inner 200 pc of our model disc: the *dashed line* is the contribution of the stars, which is assumed to rise as $R^{0.1}$; the *dotted line* is the contribution from a $10^8 M_\odot$ nuclear BH; the *solid line* is the net circular speed.

hole in M84 that is smaller than that of Bower et al. by a factor ~ 4 .

2 A SLIT WIDER THAN THE PSF

For clarity we consider long-slit spectra of a disc in circular motion in a specific but realistic axisymmetric galactic potential. We assume that the latter is generated by a nuclear BH and an extended mass distribution, in which the density varies radially as $R^{-1.8}$ – this behaviour is consistent with what is inferred for the centre of the Milky Way (Binney et al., 1991; Genzel et al., 1997) and is characteristic of the luminosity profiles of a large class of elliptical galaxies (Gebhardt et al., 1996). With the density scaling as $R^{-1.8}$, the circular speed generated by the extended mass distribution scales as $R^{0.1}$, and falls towards the centre. Consequently, there is some radius R_{BH} at which the circular speed of the embedded BH, which scales as $R^{-0.5}$, begins to dominate. The conventional approach to the determination of the mass of the BH involves fitting a Keplerian circular-speed curve to the observed rotation curve well inside R_{BH} . We shall see that with a wide slit mass inside R_{BH} can be derived from data taken at $R \simeq R_{\text{BH}}$. The ability to work near R_{BH} rather than well inside it is important because R_{BH} is typically very small — usually smaller than atmospheric seeing.

Fig. 1 shows the circular speeds out to 200 pc in our model: the dotted curve shows the circular speed generated by the $10^8 M_\odot$ BH, the dashed line shows that generated by the stars, and the full curve shows the net circular speed.

2.1 A slit parallel to the line of nodes

Fig. 2 is a composite position-velocity plot for 21 parallel cuts through our model galaxy. The disc has been inclined at 60° to the line of sight, and the cuts run parallel to the line of nodes. The inset at top left shows the locations of some representative cuts: the outermost cuts are dotted and the one through the nucleus is dashed. Velocities along the cuts

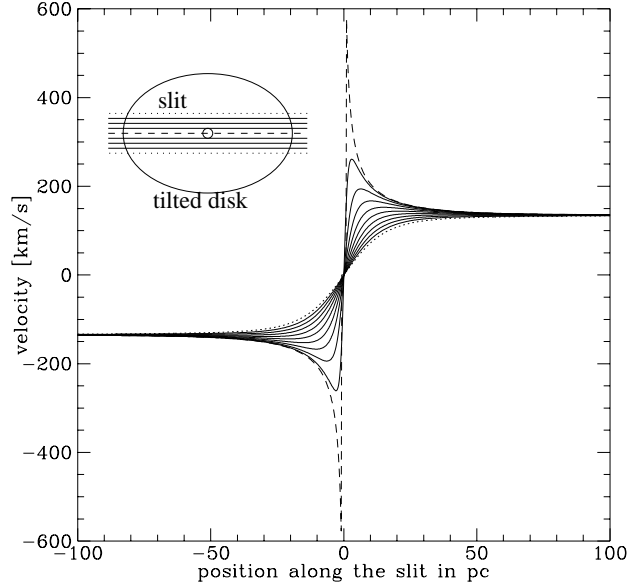


Figure 2. Position-velocity diagram for the disc described by Fig. 1 when it is viewed at inclination angle $i = 60^\circ$. Velocities are sampled along 21 cuts parallel to the line of nodes. They are symmetric with respect to the nucleus, hence only 11 lines are displayed. The cuts are represented in the inset at upper left, with the cut through the nucleus dashed, and the outermost cut, which passes $20 \cos^{-1} i$ pc from the nucleus, dotted.

differ markedly near the centre since only the cut through the nucleus fully samples the central divergence of the BH's circular-speed curve. Velocities along many outer cuts show no rise, but smoothly decline to zero at the slit centre.

2.2 Velocity offsets

When our disc is observed in some emission line through a long-slit spectrograph, the pattern of intensity resembles Fig. 2 but with some significant differences, which we now deduce by considering how the spectrograph works.

Fig. 3 shows the relevant geometry. The telescope creates an image of the disc in the slit, and we show two rays of wavelength λ through each of two points on this image: one at the centre of the slit, which lies on the optical axis, and one off-centre. After passage through the collimator, rays through the centre of the slit run parallel to the optical axis until they hit the grating, whose normal makes angle ϕ with the axis. The interference pattern produced by the grating peaks at angle θ_0 to the grating's normal, where θ_0 satisfies the diffraction equation

$$\sin \theta_0 - \sin \phi = m\lambda / \Delta, \quad (1)$$

with m being the spectral order, and Δ the row separation.

The rays going through a point on the image that is offset by δ from the centre of the slit are inclined at angle ψ to the optical axis after passing the collimator, where

$$\psi = \delta \frac{f_{\text{telescope}}}{f_{\text{collimator}}}. \quad (2)$$

Hence, their angle of incidence on the grating is $\phi - \psi$, and

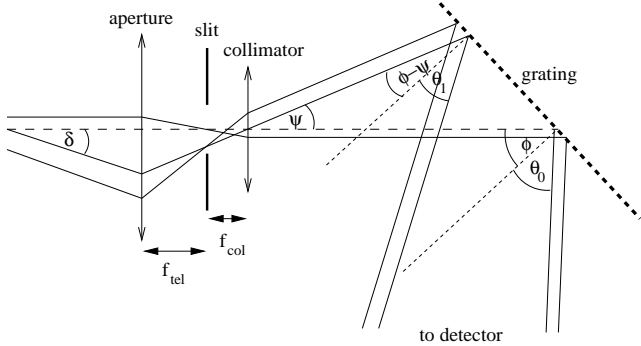


Figure 3. Paths through an ideal spectrograph of rays associated with two points on the image of an astronomical object. One ray runs along the optical axis (long-dashed line), and contributes to a maximum intensity in the direction θ_0 relative to the grating. A ray through an image point that lies distance δ from the axis contributes to an intensity maximum at angle θ_1 relative to the grating. Short-dashed lines mark normals to the grating.

the diffraction pattern to which they contribute peaks at the angle θ_1 that satisfies

$$\sin \theta_1 - \sin(\phi - \psi) = m\lambda/\Delta. \quad (3)$$

The angle θ of the peak in the diffraction pattern always decreases with the displacement δ of the source from the slit centre.

The spectrograph's camera gathers all light that enters in a given direction onto a single point on the detector. Since the on- and off-centre rays enter at different angles, they are gathered to different points on the detector despite their common wavelength. In so far as we associate a velocity with each position along the dispersion direction, we have to recognize that the velocity scale for a point distance δ from the centre of the slit is offset from the scale for the centre of the slit by an amount proportional to δ . This offset depends on wavelength λ , and is listed for individual spectrographs as a 'plate scale' (see Table 5 in Woodgate et al. 1998 for STIS). This feature of a spectrograph is commonly known as a slit effect (see e.g. Bacon et al. 1995).

For the spectral order $m = 1$, the angle θ at which constructive interference peaks increases with wavelength λ , or decreases with emitter's velocity. As noted above, it also decreases as one moves up the slit in Fig. 2. Out of convenience, we convert decrements in θ to increments in the dispersion coordinate on the detector, so that higher velocity of the emitter reveals itself as larger value of the dispersion coordinate. With this conversion, also the velocity offset is positive for points above the centre of the slit, and negative below. Fig. 4 shows the resulting pattern of light on the detector for the top half of the slit: each line from Fig. 2 is shifted by a constant amount, different for each line. As in Fig. 2, the dashed curve comes from the cut through the nucleus, and the dotted curve marks the edge of the slit, which is 2δ wide. On the left side of Fig. 4 the dotted curve is shifted up away from the dashed one, so the light is diffused over the detector in an unhelpful way. On the right side of Fig. 4, by contrast, the shift moves the dotted curve past the dashed curve at large distances along the slit, while at small distances, the shift leaves the dotted curve below the dashed curve. On this side, the instrumental velocity offset

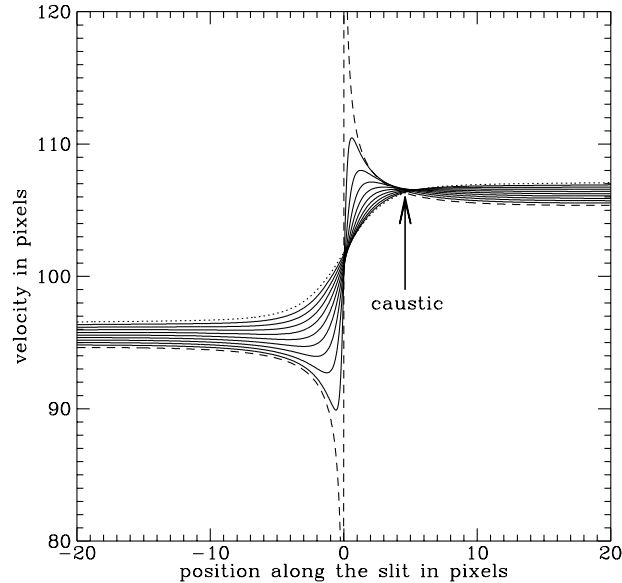


Figure 4. The distribution of light on the spectrograph's detector for a position-velocity diagram like that of Fig. 2. For clarity only the top half of the slit is sampled – velocity offsets lift the degeneracy between the velocities coming from above and below the nucleus in Fig. 2. A caustic to the right of the nucleus is marked with an arrow. The pixel scale is for a slit 0.2 arcsec wide and the G750M grating on STIS with the model disc placed at a distance of 20 Mpc.

competes with the real rise in velocity due to the nuclear BH. Close to the nucleus, the BH-related velocity rise dominates, hence the dashed line that goes through the nucleus stays on top. Further from the nucleus, the real velocity gradient across the slit is small, and the instrumental velocity offset, largest for the edge of the slit, takes over: hence there the dotted line is on top. Somewhere in between, there is a point along the slit at which the BH-related velocity rise is balanced by the velocity offset, and the dashed and dotted lines intersect. Since the curves generated by intermediate cuts are similarly shifted, the dashed curve crosses all the other curves, and happens to do so in a narrow range of distances along the slit. All light entering that part of the slit gets focused virtually at one position in the dispersion direction. We refer to this region of inversion of the order of the curves as the 'caustic'.

In the lower half of the slit, the velocity offset is negative, so the light distribution on the detector from this half of the slit is the same as that shown in Fig. 4 rotated by 180° . Fig. 5 shows the light distribution from the two halves of the slit combined. The top panel is similar to Fig. 4 except that a grid of pixels has been overlaid – the grid is appropriate for the G750M grating on STIS with the model at a distance ~ 20 Mpc, so that 1 arcsec corresponds to 100 pc. The bottom panel shows the light distribution in those pixels under the assumption that the surface brightness within the disc scales as R^{-1} .

Inside the two caustics, the light distribution shows two maxima in the dispersion direction: the one furthest from the systemic velocity is created by light coming from the slit

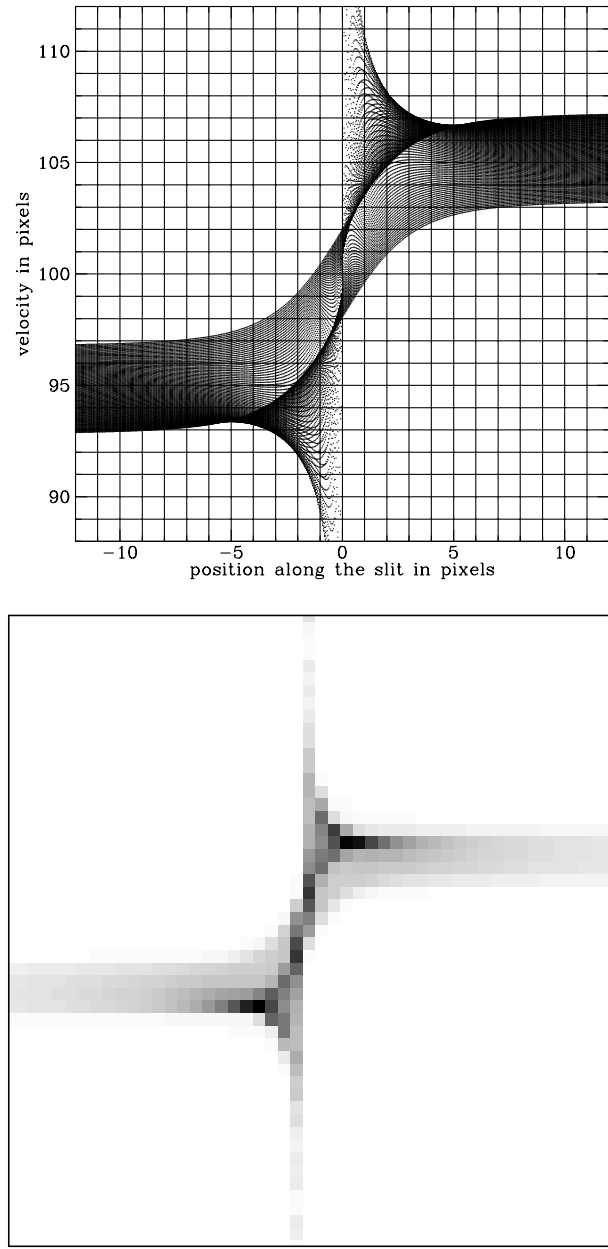


Figure 5. The light distribution on the detector of an ideal spectrograph with a wide slit as in Fig. 4, but including light from both above and below the nucleus. Top panel: light from the disc is sampled at points uniformly distributed within the slit, and for each point a dot is generated at the location of maximum intensity in the diffraction pattern. Bottom panel: the light distribution when the emission in the nuclear disc scales with radius as $\sim R^{-1}$ and light has been integrated within the detector's pixels.

centre, and contains information about the BH. The other one, made by light from slit edges, goes through zero velocity at the nucleus. Thus we predict full two-dimensional position-velocity diagrams for rotating discs to be rich in structure; the information contained in this structure is lost if one merely fits a Gaussian emission line profile at each radius (which is the traditional approach).

3 A NEW BH MASS ESTIMATOR

Observationally, the caustic described in the last section will be conspicuous because light from right across the slit is concentrated in it. We experimented with various stellar mass distributions other than the one resulting in velocity $\sim R^{0.1}$ presented here, and the position of the caustic along the slit does not depend sensitively on the stellar density profile. Any reasonable mass distribution produces caustics at locations similar to the case of no stellar mass at all. Hence, we can infer the mass of the BH from the location of the caustics.

The velocity field in the disc due to the BH is

$$v = AR^{-1/2}, \quad (4)$$

where A is related to the BH mass M_\bullet by $A = \sqrt{GM_\bullet}$. Let (α, β) be Cartesian coordinates on the sky, with β constant along the line of nodes, and let d be the distance to the system. Then the line-of-sight velocity along a cut offset from the nucleus by distance β and parallel to the line of nodes is

$$v_{\alpha\beta} = \frac{A \alpha \sin i}{d^{1/2} \left(\alpha^2 + \left(\frac{\beta}{\cos i} \right)^2 \right)^{3/4}}. \quad (5)$$

Taking the ratio of velocity $v_{\alpha 0}$ at the slit centre ($\beta = 0$) to that, $v_{\alpha\delta}$, at the slit top edge ($\beta = \delta$) for a given position α along the slit returns the value of inclination angle i

$$\cos i = \frac{\delta}{\alpha \sqrt{(v_{\alpha 0}/v_{\alpha\delta})^{4/3} - 1}}. \quad (6)$$

It is easiest to estimate the ratio $v_{\alpha 0}/v_{\alpha\delta}$ at the caustic: through a spectrograph of dispersion D (in pixel/km s $^{-1}$) and slit half-width δ , the light from the slit centre is detected at a position $Dv_{\alpha 0}$ in the dispersion direction, and the light from the slit top edge is detected at $Dv_{\alpha\delta} + B\delta$, where B is the detector plate scale in the dispersion direction (in pixel/arcsec). Thus although always $v_{\alpha\delta} < v_{\alpha 0}$, the instrumental velocity offset $B\delta$, positive for the top half of the slit, moves the light from the slit edge up towards the light from the slit centre that is emitted at higher intrinsic velocity. If the caustic occurs distance α along the slit from the nucleus, one has

$$y \equiv Dv_{\alpha 0} = Dv_{\alpha\delta} + B\delta, \quad (7)$$

where y is the position of the caustic in the dispersion direction. Therefore $v_{\alpha\delta}/v_{\alpha 0} = 1 - \frac{B\delta}{y}$ and (6) expressed in observable quantities takes the form

$$\cos i = \frac{\delta}{\alpha} \left(\left(1 - \frac{B\delta}{y} \right)^{-4/3} - 1 \right)^{-1/2}. \quad (8)$$

The mass of the BH can now be calculated by inserting this value of i in (5) for $\beta = 0$. We find

$$M_\bullet = \frac{\alpha d}{G} \left(\frac{y}{D \sin i} \right)^2. \quad (9)$$

We have checked the usefulness of these formulae by using them to analyse the realistic spectrum shown in the bottom panel of Fig. 5. The caustic occurs at the fourth pixel along the slit from the nucleus, and is located at the seventh pixel in the dispersion direction. These numbers yield $i = 50^\circ$ and $M_\bullet = 2.6 \times 10^8 M_\odot$ compared to the input values $i = 60^\circ$ and $M_\bullet = 10^8 M_\odot$. The errors here are dominated by the neglect in the above derivation of the stellar

mass distribution which is unknown. They can be reduced by recalling that the position of the caustic along the slit, α , is fairly independent of the stellar density profile, but its position in the dispersion direction, y , is sensitive to the stellar density profile because it measures the mass interior to α . The calculations above should have used the position of the caustic y_\bullet when the BH acts alone. From equation (7) we have that $y/y_\bullet = v_0(\alpha)/v_\bullet(\alpha)$, where $v_\bullet(\alpha)$ is the velocity due to the BH alone. Let $v_*(\alpha)$ be the velocity due to the stars, then

$$y = y_\bullet \sqrt{1 + \left(\frac{v_*}{v_\bullet}\right)^2}. \quad (10)$$

Setting $v_*/v_\bullet = 1$ (see Figs. 1 and 4), we get $i = 66^\circ$ and $M_\bullet = 0.86 \times 10^8 M_\odot$ in good agreement with the input values.

The key advantage of this technique for determining M_\bullet is that it exploits a feature that occurs at the outer edge of the BH's sphere of influence, and therefore gives higher sensitivity to BH detection than the traditional method, in which one fits the Keplerian rise of the rotation curve at the smallest accessible radii. Moreover, our approach yields the mass of the black hole and the disc inclination independently, whereas the traditional approach only yields $M_\bullet \sin^2 i$. One should keep in mind though that our method yields the mass within the radius of the caustic, and to get the BH mass one must assume the contribution to the potential from extended mass. This method cannot determine whether the measured mass comes from the BH, but on the other hand the very existence of the caustic comes from the steep velocity rise towards the nucleus, which itself is characteristic of a massive BH. Thus the main advantage of our technique is in detecting BHs in galaxies for which we cannot achieve the resolution required to follow the Keplerian rise in velocities inwards.

4 INCLINED SLITS

Since nuclear discs frequently lie in a plane that differs markedly from that of galaxy's main disc, one usually does not know the line of nodes before nuclear spectra are taken. Hence, we now consider a slit that passes through the nucleus at an arbitrary position angle (PA) with respect to the line of nodes.

The top panel of Fig. 6 is the analogue of Fig. 2 for the case of non-zero PA: it is a position-velocity plot for several cuts that are inclined at $PA = 40^\circ$ to the line of nodes. The dashed curve is for the cut that passes through the nucleus, and the other cuts all pass above the nucleus. Notice that this plot, unlike Fig. 2, is not symmetric on inversion through its centre; the plot one obtains by carrying out this inversion is the position-velocity plot for cuts that pass below the nucleus.

The middle panel of Fig. 6 is the analogue of the top panel of Fig. 5 for non-zero PA. It shows the effect of adding the velocity offsets associated with finite slit width to the velocities shown in the top panel, together with the corresponding velocities for the cuts below the nucleus.

The bottom panel is the analogue of the middle panel for a disc that rotates in the opposite sense: thus before

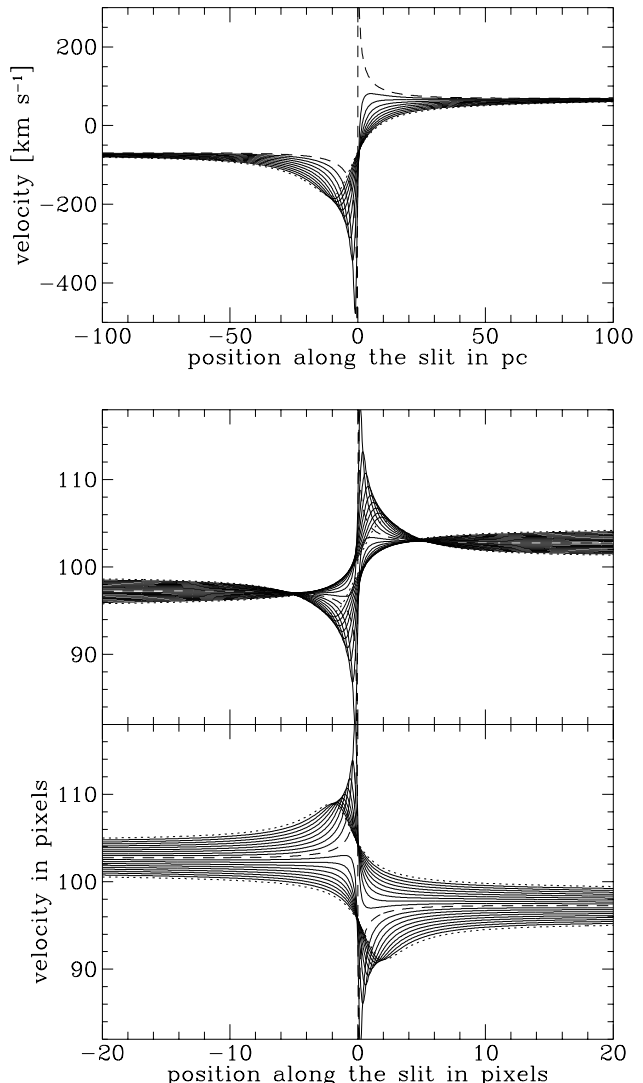


Figure 6. The effect of non-zero angle ($PA = 40^\circ$) between the slit and the line of nodes. Top panel: the position-velocity diagram for the upper half of the slit, as in Fig. 2 – velocities for the lower half can be obtained by inverting the diagram through its centre. Middle panel: the distribution of light on the spectrograph's detector, as in Fig. 5. Bottom panel: the same but for a disc that rotates in the opposite sense.

adding the velocity offsets we changed the sign of the velocities given by the top panel. Clearly the bottom and middle panels differ by much more than a reflection. In particular, one has prominent caustics on the spatial axis while the other does not. Given that these two panels describe observations with the same spectrograph of systems that differ only in their sense of rotation, the striking differences between these panels may be surprising. They reflect the fact that a spectrograph is symmetric only under inversion of both the spatial and temporal axes, and not symmetric under time reversal only. The latter asymmetry is evident because a spectrograph displays frequency shifts as spatial displacements. For the same reason, changing the sense of rotation of the disc is equivalent to switching the sign of the observed spectral order (see eq. 1).

When the slit lies along the line of nodes, cuts that pass $\pm\delta$ above and below the slit map to the same point in the position-velocity plot at a given distance down the slit (see Fig. 2). Consequently, it is immaterial whether contributions coming from above the nucleus are moved up and the others down, or vice-versa. When the slit does not run along the line of nodes, cuts above and below the nucleus map to different points in the position-velocity plot, and it matters which is moved up and which down.

Although the appearance of the spectrum changes with the slit position angle, the principal features persist. In the middle and bottom panels of Fig. 6, one can see the caustics, and two intensity maxima inside the caustics. Notice that, whereas in Fig. 5 the outer envelope of the light distribution near the nucleus is formed by light coming through the slit centre, in Fig. 6 it comes from the sides of the slit – the dashed line associated with the slit centre has a much narrower peak. Consequently, fitting profiles from an infinitely thin slit to the light distributions in the lower panels of Fig. 6 would result in a considerable overestimation of the BH mass when the traditional method is being used. We give an example of this phenomenon in Section 6.

Our method relies on the existence of caustics to diagnose the presence of a BH. Since Fig. 6 shows that for non-zero PA the appearance of caustics can depend on the sense of disc rotation, it follows that the detectability of a BH with a given spectrograph setup depends on the sense of rotation of its accretion disc. As the slit position angle increases, the caustic becomes more difficult to detect as it moves in to the nucleus and often to higher velocities.

With unknown PA, our method returns only two out of three parameters: PA, i , M_\bullet . However, equations (6) to (9) are readily generalized to the case of non-zero position angle. Equation (5) gives the line-of-sight velocity at a point (α, β) in the disc, with $\beta = 0$ marking the line of nodes through the nucleus. For a cut inclined at a given PA, the coordinate α' down the slit, and the offset β' of the cut are related to (α, β) by a simple rotation matrix

$$\alpha' = \alpha \cos \text{PA} - \beta' \sin \text{PA} \quad (11)$$

$$\beta' = \beta' \sin \text{PA} + \beta' \cos \text{PA}. \quad (12)$$

Substituting these values of (α, β) into equation (5) gives the velocity v_0 in the nuclear cut ($\beta' = 0$), and $v_{\pm\delta}$ in the cut marking the edge of the slit ($\beta' = \pm\delta$). As in (6), the inclination angle can be recovered from the ratio $v_0/v_{\pm\delta}$:

$$\cos^2 i = \frac{\Gamma^{4/3}(\sin \text{PA} \pm \frac{\delta}{\alpha} \cos \text{PA})^2 - \sin^2 \text{PA}}{\cos^2 \text{PA} - \Gamma^{4/3}(\cos \text{PA} \mp \frac{\delta}{\alpha} \sin \text{PA})^2}, \quad (13)$$

where

$$\Gamma = \frac{v_{\pm\delta}}{v_0} \left(1 \mp \frac{\delta}{\alpha} \tan \text{PA} \right)^{-1}, \quad (14)$$

and the prime has been dropped from α for simplicity. In equations (13) and (14), the upper sign refers to the top edge of the slit, and the lower sign to the bottom edge – this dichotomy reflects the loss of the symmetry that takes place as the PA is displaced from zero. From equation (7) we again get $v_{\pm\delta}/v_0 = 1 \mp \frac{B\delta}{y}$. Substituting this ratio into equation (14) we obtain an expression for the inclination in terms of observed quantities. The mass of the black hole can then be obtained from equations (5) and (11) with $\beta' = 0$:

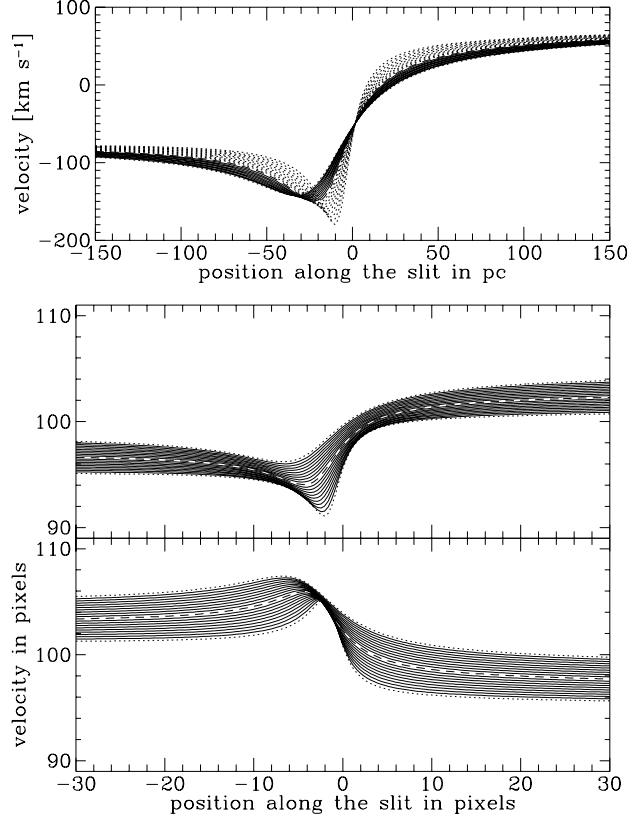


Figure 7. The same as Fig. 6 but with the centre of the slit displaced by the slit width, 0.2 arcsec, from the nucleus. The outer dotted lines sample the slit edges, the dashed ones the slit centre. The top panel is a position-velocity plot, with additional set of dotted lines sampling the bottom half of the slit. The middle and bottom panels show the light distributions in the spectrograph's detector for discs rotating in opposite senses.

$$M_\bullet = M_\bullet(\text{PA} = 0) \frac{(1 - \cos^2 \text{PA} \sin^2 i)^{3/2}}{\cos^3 i \cos^2 \text{PA}}, \quad (15)$$

where $M_\bullet(\text{PA} = 0)$ is given by equation (9). Note that the correction factor in the equation above quickly diverges for $i \rightarrow 90^\circ$ and $\text{PA} \rightarrow 90^\circ$, but otherwise it remains a mild function of i and PA. In Section 6, we use published data and these formulae to obtain a new estimate of the mass of the BH in M84.

4.1 Offset Slits

It is a common strategy to use offset slits to recover the PA of the nuclear disc, and to disentangle values of M_\bullet and i from the value of the product $M_\bullet \sin^2 i$ that emerges from the conventional treatment of a slit through the nucleus. We have shown how this disentanglement can already be done directly from data for a wide slit through the nucleus, and it is a priori evident that a proper treatment of wide slits greatly reduces the value of offset slits: a wide slit through the centre already contains a narrow off-set slit. Constraints on the disc PA can be inferred from offset slits, and there are a couple of features of offset slits that merit mention.

First, the pattern of light on the detector is the same for slits that pass equal distances above and below the nu-

cleus. Fig. 7 is the analogue of Fig. 6 for an offset slit – the PA is still 40° but now the centre of the slit misses the nucleus by 0.2 arcsec. Again we see that the light distribution in the detector differs qualitatively depending on the sense of rotation of the disc. The bottom boundary of the light distribution in the two lower panels of Fig. 7 is set by light from the edge of the slit that passes closest to the nucleus. The nuclear BH causes a mere widening of the light pattern close to the galactic centre in the middle panel, while in the lower panel a caustic is evident. This panel corresponds to the same sense of rotation as the bottom panel in Fig. 6, in which there is no comparable concentration of light. Hence, when the disc rotates in the least favourable sense for black hole detection with a slit through the nucleus, this is the favoured sense of rotation for detection from an offset slit.

Finally, fitting the thin-slit model to the off-center data again results in an overestimate of the BH mass: The disc's intensity will be highest along the edge of the slit that passes closest to the nucleus. In the two lower panels of Fig. 7 this edge forms the lower dotted line. Since the curvature of this line is larger than the curvature of the dashed central line, the BH mass will be overestimated if the curvature of the light profile serves as the BH-mass estimator.

5 CONVOLUTION WITH THE PSF

The discussion above has been confined to the distribution of the principal maxima in the diffraction pattern that is produced on the spectrograph's detector by light of a given frequency coming from a given point in the object being measured. In reality light from a point on the target is distributed over the slit by the PSF of the primary telescope optics, and light from any point on the slit produces an entire diffraction pattern on the detector. To what extent would our conclusions be modified if we took into account the complete diffraction pattern?

We cannot answer this question rigorously for lack of sufficient data on STIS. To see what data are required, recall that light at a given frequency from a given point on the object is concentrated by the primary telescope optics into an interference pattern in the plane of the slit. Ideally, this pattern would comprise an Airy disc and rings, but it is in reality complex. The slit truncates this pattern. After passage through the spectrograph, light from every surviving point in the pattern interferes both with itself and light from other surviving points in the pattern, so in principle one needs to know the phase of the radiation within the slit and not just the intensity pattern.

Here we neglect the effects of the coherence of radiation at different points in the slit, and add contributions from truncated Airy discs in intensity – this is strictly correct only in the case of a seeing-dominated PSF. For each point in the source we approximate the Airy pattern in the slit plane with the circular model PSF. We chose the PSF obtained by Roeland van der Marel (2000, private communication) from tests on STIS that involved shifting a star across a 0.1 arcsec-wide slit. This PSF is approximated by four Gaussians

$$\text{PSF}(r) = \sum_{i=1}^4 \frac{\gamma_i}{2\pi\sigma_i^2} \exp(-r^2/2\sigma_i^2), \quad (16)$$

Table 1. Parameters of PSF model for STIS

i	γ_i	σ_i (arcsec)
1	0.219954	0.019070
2	0.599261	0.041687
3	0.147840	0.172908
4	0.032945	0.580370

with parameters listed in Table 1. It has a FWHM of 0.057 arcsec. Its pattern is truncated by the slit edges. The light from each surviving point on a given Airy disc is propagated to the detector according to equation (3), *i.e.* it is placed at the maximum of the diffraction pattern. This approach recovers the flux on the detector and the velocity offset measured in the abovementioned set of tests, and therefore gives a faithful approximation of the light pattern on the detector. In the next section, we confront our models, already convolved with the PSF, with the STIS data.

6 CONFRONTING OBSERVATIONS

To date, the most unambiguous gas kinematical detection of a nuclear BH with STIS is that for M84 by Bower et al. (1998). The left panel of Fig. 8 shows the relevant spectrum, which was taken with a slit 0.2 arcsec wide. At several positions just to the right of the nucleus, the emission clearly peaks at two velocities. Consequently, when Bower et al. fitted Gaussians in velocity to the data, they found two Gaussians to be required at many spatial locations. Bower et al. interpreted this finding in terms of two gas components. Fig. 5 shows that when the non-negligible width of the slit is taken into account, two peaks arise naturally from the simplest model of the accretion disc, in which there is a unique velocity at a given radius.

In the left panel of Fig. 8 we interpret the point – ~ 0.45 arcsec (nine pixels) from the nucleus – at which the track of maximum light splits into two, as the position of the caustic. We estimate the corresponding velocity to be 125 km s^{-1} . Adopting the Bower et al. value of the relative position angle of the slit with respect to the line of nodes (PA = 21°), and roughly accounting for the stellar mass contribution, we derive $i = 74^\circ$ and $M_\bullet = 4 \times 10^8 M_\odot$ from equations (13) and (15). Our estimate of i agrees roughly with that of Bower et al. ($i = 80^\circ$), but our value for M_\bullet is almost 4 times smaller than that of Bower et al. We believe the Bower et al. value is too large because it is based on fitting a thin slit model to the outer envelope in light distribution, which is dominated by light from the edge of the slit. In Section 4 we showed how this procedure can lead to a significant overestimation of M_\bullet .

The observed spectrum is distinctly left-right asymmetric, which makes it different from a generic model in Fig. 5. Any failure to get the centre of the slit to pass through the nucleus will inevitably introduce such asymmetry. We therefore simulated a STIS spectrum for $M_\bullet = 4 \times 10^8 M_\odot$, $i = 74^\circ$ and relative PA = 21° , and the centre of the slit displaced from the nucleus by 0.03 arcsec, less than a quarter of its width. The middle panel of Fig. 8 shows the light distribution on the detector after convolution with the PSF;

in the right panel, this light has been binned into pixels. The simulated spectrum clearly reproduces the main features of the observed spectrum next to it: on the left-hand side of this spectrum, the BH-related rise in velocities is clear, with not much emission in the second light maximum at low velocities. On the other hand, most of the light on the right of the nucleus is gathered into the low-velocity maximum, with the emission from the BH-related velocity rise enhanced only close to the galactic centre. All emission recorded in the nuclear slit spectrum observed by Bower et al. can be explained as coming from a thin disc in circular motion around the central BH. Note that although the distribution of intensities changes when the slit is displaced, the relative position of caustics remains unchanged.

It is also worth noting that the convolution with PSF does not introduce any significant change in the light pattern on the detector already outlined in Fig. 5. It is so because the slit width considered here (0.2 arcsec) is substantially larger than the FWHM of the instrumental PSF. Thus in observations with a sufficiently wide slit, the convolution with the PSF can be treated as a small correction to the slit effects described in this paper.

Since our analysis of spectra taken with a wide slit is motivated by a program of STIS observations, we have confronted our simulated spectra with the STIS observations of Bower et al. (1998). However, the effects of a wide slit already may be evident in older spectra of M87 that were taken with the Faint Object Camera on HST (Macchetto et al. 1997). Two bright spots located symmetrically on each side of the nucleus and separated by a drop in the emission in the innermost 0.1 arcsec may indicate the presence of caustics, but we cannot make a strong case here because of limited quality of the data.

7 CONCLUSIONS

We have analysed the consequences of using a long-slit that is significantly wider than the PSF of the primary telescope optics. When the object under study contains large velocity gradients, such that the object's velocity can change appreciably across the slit, the pattern of light that will be measured on the detector differs qualitatively from what one would observe with an ideal narrow slit. There is more information in a spectrum taken with a wide slit than in a spectrum of equal S/N that is taken with a narrow slit. This happy state of affairs in natural intuitively, since a wide slit contains many narrow slits within it.

Competition between real velocity differences within the object, and offsets in velocity that arise because light from different points across the slit enter the spectrograph at different angles, frequently cause the intensity of light on the detector to have more than one peak at a given spatial location, even for a trivial velocity field in the object. Such multiple peaks in spectra of galactic nuclear discs have already been observed from the ground (*e.g.* Rubin, Kenney & Young 1997), and are evident in STIS spectra (Bower et al. 1998). In this last observation, they were interpreted as evidence for multiple components along a single line of sight. Bertola et al. (1998) showed that this does not need to be the case, and serious physical problems are likely to be encountered when a three-dimensional model is sought that

displays such components. Here we confirm this finding, and in addition conclude that, when correctly interpreted, the multiple peaks have considerable diagnostic power: they enable us to detect nuclear black holes by exploiting data for a given galaxy at larger distances from the nucleus than in the traditional approach to BH mass-estimation. Our BH-detection method is therefore reliable down to lower black-hole masses (M_\bullet) for which detection of Keplerian rise of velocity inwards is beyond the resolution limit. Moreover, our estimator recovers M_\bullet and the inclination i of the disc independently from a single long-slit spectrum, whereas from the same spectrum the traditional approach determines only the value of the product $M_\bullet \sin^2 i$ and requires an additional spectrum from an off-set slit to extract M_\bullet and i separately from the product. Nevertheless we ought to point out that our method serves only as a rough indicator of a central mass concentration, and tells us nothing about the mass distribution inside the caustic. The traditional method that follows the Keplerian rise in velocities will secure the BH detection once data with sufficient resolution become available.

When the slit is inclined at some angle to the line of nodes, the distribution of light on the spectrograph's detector differs qualitatively depending on the sense in which the disc rotates. Consequently, with a given spectrograph setup, the detectability of a black hole depends on the sense in which the disc surrounding it rotates.

We applied our mass estimator to a published spectrum of M84 (Bower et al. 1998), and find that in this galaxy M_\bullet is 4 times smaller than previously estimated. We argue that interpretation of data taken with a wide slit in terms of an infinitely thin slit will cause M_\bullet to be systematically overestimated. Currently we are estimating the masses of nuclear BHs in a sample of ~ 50 nearby galaxies for which we have STIS spectra (Marconi et al. 2000, Axon et al. 2000).

ACKNOWLEDGMENT

We would like to thank Gary Bower for providing us with the data shown in Fig. 8 and Roeland van der Marel for providing us with unpublished test data for STIS, and for useful comments.

REFERENCES

- Axon D.J. et al. , 2000, in preparation
- Bacon R. et al. , 1995, *AApS*, 113, 347
- Baum S. et al. , 1996, STIS Instrument Handbook, Version 1.0 (Baltimore: STScI)
- Bertola F., Cappellari M., Funes J.G., Corsini E.M., Pizzella A., Vega Beltran, J.C., 1998, *ApJ*, 509, L93
- Binney J., Gerhard O. E., Stark A. A., Bally J., Uchida K. I., 1991, *MNRAS*, 252, 210
- Bower G.A. et al. , 1998, *ApJ*, 492, L111
- Copin Y. et al. , 2000, in Combes F. et al., eds, *ASP Conf. Ser.* Vol. 197, *Dynamics of Galaxies: From the Early Universe to the Present*. Astron. Soc. Pac., San Francisco, p.249
- Gebhardt K. et al. , 1996, *AJ*, 112, 105
- Genzel R., Eckart A., Ott T., Eisenhauer F., 1997, *MNRAS*, 291, 219
- Macchetto F., Marconi A., Axon D.J., Capetti A., Sparks W., Crane P., 1997, *ApJ*, 489, 579

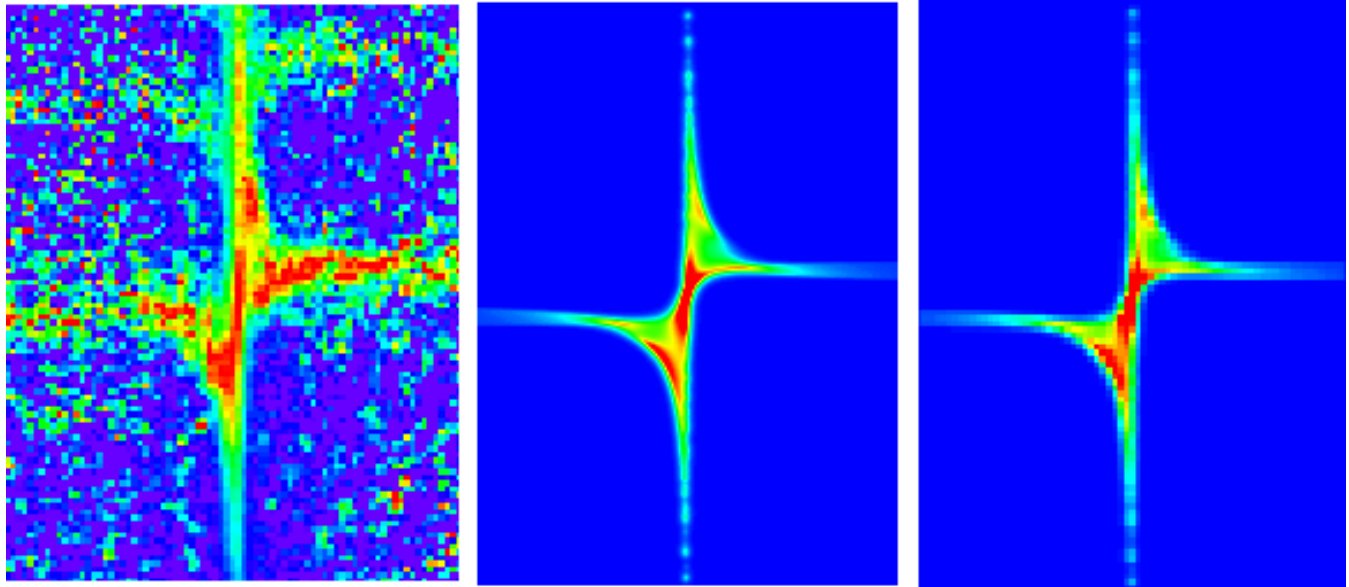


Figure 8. Left: an $H\alpha$ emission-line spectrum of M84 taken with STIS using the G750M grating (from Bower et al. 1998). The dispersion direction is vertical. Centre: a modeled light distribution on the spectrograph's detector (convolved with instrumental PSF) for $i = 74^\circ$, $PA = 21^\circ$, $M_\bullet = 4 \times 10^8 M_\odot$, and the centre of the slit shifted by 0.03 arcsec from the nucleus. The distance to M84 has been taken to be 17 Mpc and the surface-brightness of the emission has been assumed to be proportional to $R^{-1.5}$. Right: light distribution from the central panel integrated over detector pixels.

Marconi, A. et al. , 2000, in Galaxies and their Constituents at the Highest Angular Resolution, Proc. IAU Symposium 205
 Rubin V.C., Kenney J.D.P, Young J.S, 1997, AJ, 113, 1250
 Woodgate B.E. et al. 1998 PASP 110, 1183